International Journal of Solids and Structures 49 (2012) 3816–3822

Contents lists available at SciVerse ScienceDirect

International Journal of Solids and Structures

journal homepage: www.elsevier.com/locate/ijsolstr

Design of nonlinear springs for attaining a linear response in gap-closing electrostatic actuators

Ben Rivlin, David Elata *

Faculty of Mechanical Engineering, Technion, Israel Institute of Technology, Haifa 32000, Israel

ARTICLE INFO

Article history:
Received 27 February 2012
Received in revised form 30 July 2012
Available online 29 August 2012

Keywords:
Nonlinear springs
Electrostatic actuation
Gap-closing electrostatic actuators

ABSTRACT

Gap-closing electrostatic actuators are inherently nonlinear and their dynamic range is often limited by the pull-in instability. To overcome this, we propose a nonlinear spring that counteracts the nonlinear effects of electrostatic attraction. The nonlinear spring is designed to extend the stable range of the actuator and to enforce a linear electromechanical response. We present a method for designing elastic springs with monotonically increasing stiffness. The mechanism we propose is effective shortening of a straight clamed-guided beam flexure, by wrapping it over a cam. We consider two specific cases. The first case assumes the wrapped section of the beam flexure fully conforms to the cam shape. The second case assumes that there is a single contact point between the beam flexure and the cam. To validate the concept we have designed and measured the response of a nonlinear spring with a prescribed force–displacement law. Experimental measurements of a macro-scale spring are in good agreement with the model predictions.

1. Motivation

Electrostatic actuators are prevalent in MEMS because they are efficient at the micro-scale and because they are compatible with microfabrication technology (Liu, 2006; Madou, 2011; Maluf and Williams, 2004). The simplest electrostatic actuator is the gap-closing parallel-plates actuator, schematically illustrated in Fig. 1a. A variable capacitor is constructed from a movable plate-electrode of area A which is suspended on an elastic spring with stiffness k over a fixed electrode. The movable plate-electrode has a single degree-of-freedom Δ, and the initial gap between the plates is g. The top electrode is subjected to a driving voltage V and the bottom plate is grounded.

Ignoring fringing fields, the equilibrium equation of the system is (Elata, 2006)

$$f_m = \frac{1}{2}\frac{\varepsilon_0 A}{(g-\Delta)^2}V^2 \tag{1}$$

where f_m is the mechanical restoring force in the elastic spring and ε_0 is the permittivity of free-space. The stiffness of the system is given by

$$K = k - \frac{\varepsilon_0 A}{(g-\Delta)^3}V^2 \tag{2}$$

where $k = df_m/d\Delta$. In many mechanical systems elastic springs are intended to be linear (i.e., $k = const.$) but inevitable nonlinearities often result in unexpected effects (e.g. (Osterberg and Senturia, 1997; Younis and Nayfeh, 2003)). If indeed we assume a linear spring in the system described in Fig. 1a, then the equilibrium equation and system stiffness (at equilibrium) are given by

$$k\Delta = \frac{1}{2}\frac{\varepsilon_0 A}{(g-\Delta)^2}V^2 \tag{3}$$

$$K = k\frac{g-3\Delta}{g-\Delta} \tag{4}$$

The equilibrium response curve is plotted in Fig. 1b. Equilibrium displacement is evidently a nonlinear function of the driving voltage and the system becomes unstable (i.e., $K < 0$) when the displacement exceeds a critical value (i.e., $\Delta > g/3$). This critical point is the pull-in point of the system, and the pull-in voltage associated with that point is the maximal voltage that can be applied to the system before it loses its stability (Elata, 2006).

Quite a few provisions for extending the stability range of gap-closing electrostatic actuators have been proposed over the years (e.g. power-law springs (Burns and Bright, 1997), leveraged bending (Hung and Senturia, 1999), stress stiffening (Deutsch et al., 2003), charge-control actuation (Nadal-Guardia et al., 2003, 2002) and piecewise stiffening springs (Cortopassi and Englander, 2001)). But these provisions could not eliminate the nonlinear nature of the response.

* Corresponding author. Tel.: +972 4 829 3184.
E-mail address: elata@technion.ac.il (D. Elata).

0020-7683/$ - see front matter © 2012 Elsevier Ltd. All rights reserved.
http://dx.doi.org/10.1016/j.ijsolstr.2012.08.014

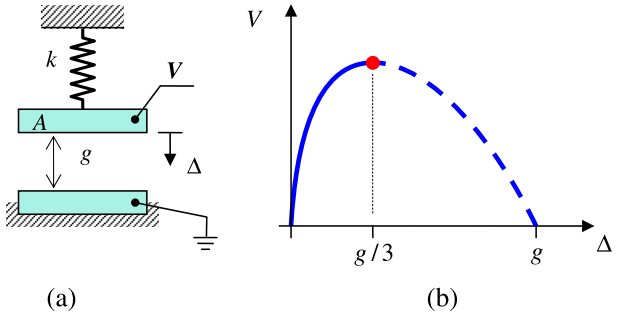

Fig. 1. (a) Schematic view of the parallel-plates electrostatic actuator. (b) The equilibrium response of the system is nonlinear; it is stable up to $\Delta = g/3$ and is unstable beyond that displacement.

A linear response curve is always coveted because calibration of linear systems is straightforward. Moreover, if the system response is linear, this linearity is often unaffected by ambient conditions (e.g. changes in temperature) although the calibration factor may be affected.

Seemingly, the ultimate solution for extending the dynamic range of electrostatic actuators is the comb-drive actuator (Tang et al., 1989). Furthermore, a double-sided comb-drive actuator with a specific driving strategy will result in a linear response (Marxer et al., 1999).

The motivation to this work is finding a way to enforce a linear response of the gap-closing parallel-plate actuator. Specifically, in view of Eq. (1), if we could find a way to produce an elastic suspension in which the mechanical restoring force takes the form

$$f_m = \frac{\beta\Delta^2}{(g-\Delta)^2} \tag{5}$$

where β is a constant, then equilibrium Eq. (1) will become

$$\frac{\beta\Delta^2}{(g-\Delta)^2} = \frac{1}{2}\frac{\varepsilon_0 A}{(g-\Delta)^2}V^2 \tag{6}$$

It is evident that in this case, displacement is linearly proportional to the driving voltage! For the force–displacement law (5), the stiffness is a monotonically increasing function of displacement (see Eq. (23) in the following).

The key question which is addressed in this paper is how to produce an elastic suspension with a monotonically increasing stiffness. The answer we propose is using cams of specific shape which effectively shorten the length of flexures as load is increased. In the past, we have used a similar concept to measure the strength of brittle microbeams without measuring any forces or displacements (Elata and Hirshberg, 2006).

In the next section we revisit the mechanical response of an elastic beam, which will serve as background. Two different design methodologies are presented in Sections 3 and 4. Application of these methodologies to the force–displacement law specified above is presented in Section 5, followed by experimental verification in Section 6.

2. Beam theory

In this work we consider suspensions that are constructed from straight elastic beams that have a rectangular cross-section. These beams are considered to deform in a given plane due to external loads, and their deflection is given by the elastica equation (Love, 1944)

$$E^* I\frac{d\theta}{ds} = M(s) \tag{7}$$

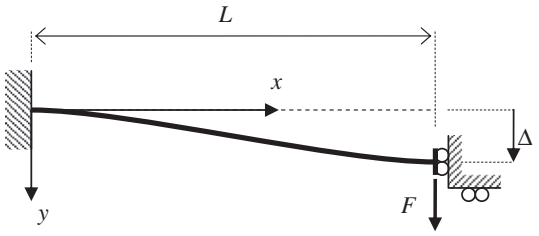

Fig. 2. A clamped-guided beam spring.

Here θ is the angle between the beam and its initial orientation in the plane, and s is a measure of distance along the beam ($0 \leqslant s \leqslant L$ where L is the beam length). $I = \frac{1}{12}bh^3$ is the second moment of the cross-section, where b is the beam width and h is the beam height. It is tacitly assumed that the beam is slender (i.e., $h \ll L$ and $b \ll L$). The effective elastic modulus for wide beams (i.e., $b \gg h$) is $E^* = E(1-\nu)^2$ where E is the Young modulus of the elastic material and ν is its Poisson ratio. Finally, $M(s)$ is the resultant bending moment at cross-section s.

For cases in which the angle of the bent beam is well in the range $(-\pi/2,\ \pi/2)$ Eq. (7) can be written in the form

$$E^* I\frac{y''(x)}{(1+(y'(x)^2)^{3/2}} = M(x) \tag{8}$$

where the fixed coordinate x is used instead of distance s along the curved beam. If the beam deflection is further limited to small angles, Eq. (8) can be further simplified to the Euler–Bernoulli beam equation

$$E^* I y''(x) = M(x) \tag{9}$$

For example, consider the clamped-guided beam illustrated in Fig. 2, which is subjected to a transverse edge force F. The edge of the beam deflects without rotation and is therefore suitable as a spring for the parallel-plates actuator. However, the guided edge does not constrain axial or transverse motion of the beam edge. The beam deflection is given by

$$y = \frac{F}{E^* I}\left(\frac{Lx^2}{4} - \frac{x^3}{6}\right) \tag{10}$$

The edge deflection is $\Delta = y(L) = FL^3/12E^*I$, and the flexure has a constant stiffness

$$k = \frac{dF}{d\Delta} = \frac{12E^* I}{L^3} \tag{11}$$

To achieve a suspension in which the edge deflection is a prescribed function of force, we have to modify at least one of the variables E^*, I, or L, as function of the edge deflection. Since it seems impractical to continuously modify E^* or I, we will modify the effective length of the beam as it bends, as presented in the next section.

3. Cam-wrapping - a mechanism for enforcing beam shortening

In order to shorten the beam as its edge displacement increases, we wrap it over a cam of a prescribed profile, while maintaining the guided end condition. In this section we show how the cam profile can be derived in order to achieve a specific force–displacement curve with monotonically increasing stiffness.

The beam of length L is initially in contact with the cam at its left edge. To facilitate the analysis, we describe the cam and the wrapped section of the beam with coordinate system (x,y) with origin at the initial contact point. The non-wrapped section of the beam is described in coordinate system (ξ,η) with origin at the guided end of the beam (Fig. 3).

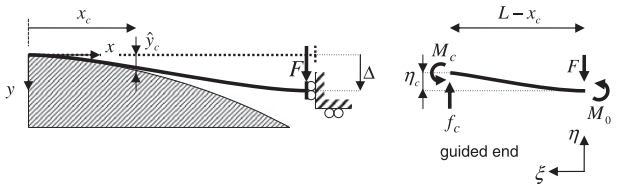

Fig. 3. Schematic model of a clamped-guided beam which is wrapped over a cam, with detail of the non-wrapped section.

When the beam is wrapped over the cam the last point of contact is x_c, and up to that point the beam is assumed to conform to the cam profile $\hat{y}(x)$ (the possibility of disconnection in the wrapped section will be discussed later). The length of the unwrapped section of the beam is therefore $L - x_c$. At the guided end, the beam is subjected to a transverse force F and a reactive moment M_0 which is required to constrain rotation.

The deflections along the unwrapped section of the beam can be determined by solving the Euler–Bernoulli beam equation (9), or alternatively if the developing deflection angles are large, the elastica equation (7) may be solved.

In either case, the boundary conditions at the guided end are

$$\eta(\xi = 0) = 0\,, \quad \left.\frac{d\eta}{d\xi}\right|_{\xi=0} = 0 \tag{12}$$

The continuity conditions at the last point of contact are

$$\left.\frac{d\hat{y}}{dx}\right|_{x_c} = \left.\frac{d\eta}{d\xi}\right|_{x_c} \text{ and } \left.\frac{d^2\hat{y}}{dx^2}\right|_{x_c} = -\left.\frac{d^2\eta}{d\xi^2}\right|_{x_c} \tag{13}$$

The second condition in (13) indicates that no external concentrated bending moment is applied at x_c. The minus sign on the right hand side of the second condition in (13) correlates the beam curvature expressed by the two coordinate systems used on the two sides of x_c.

For any value of x_c, the edge deflection Δ can be expressed as the sum of the height of the cam at x_c and the deflection of the non-wrapped section of the beam,

$$\Delta(x_c) = \hat{y}(x_c) + \eta(x_c) \tag{14}$$

Solving Eqs. (9)–(14) we find expressions for the edge force F and edge deflection Δ as functions of the point of contact for any given state of wrapping

$$F(x_c) = 2\frac{E^*I}{(L-x_c)^2}\left\{\left.\frac{d\hat{y}}{dx}\right|_{x_c} + \left.\frac{d^2\hat{y}}{dx^2}\right|_{x_c}(L-x_c)\right\} \tag{15}$$

$$\Delta(x_c) = \hat{y}(x_c) + \frac{2}{3}\left.\frac{d\hat{y}}{dx}\right|_{x_c}(L-x_c) + \frac{1}{6}\left.\frac{d^2\hat{y}}{dx^2}\right|_{x_c}(L-x_c)^2 \tag{16}$$

Since we are only interested in suspensions with monotonically increasing stiffness, we may assume that both force (15) and edge displacement (16) are monotonically increasing functions of x_c. Therefore, we can compute the suspension stiffness using the chain rule

$$k = \frac{dF}{d\Delta} = \frac{\frac{dF(x_c)}{dx_c}}{\frac{d\Delta(x_c)}{dx_c}} = \frac{12E^*I}{(L-x_c)^3} \tag{17}$$

which is compatible with (11) with the exception that the effective length of the beam is $L - x_c$.

Eqs. (15) and (16) are each a linear, second-order non-homogenous differential equation for the cam profile $\hat{y}(\hat{x})$. In Eq. (15), $\hat{y}$ does not appear explicitly, and $F(x_c)$ can be derived from the known relations of $F(\Delta)$ and Eq. (17) which relates $dF(\Delta)/d\Delta$ to the variable x_c. Eq. (16) contains both $\hat{y}$ and its derivatives and the left-hand side can once again be deduced from (17). For some functions $F = F(\Delta)$, solving Eq. (15) may be simpler than solving (16), whereas for others it may be harder. Nevertheless, both equations yield the same solution (once the initial conditions for integration have been set).

After the cam shape has been obtained, there are three things that have to be verified. The first verification is ensuring that the maximal stress induced in the flexure does not exceed a permissible value (i.e., measure of strength). The second verification is that the Euler–Bernoulli approximation is sufficient (i.e., $d\hat{y}/dx, << 1$). This issue may be cleared by either simulating the wrapping using the elastica equation (7), or alternatively by using the elastica equation at the outset to design the cam (this option is not discussed in the present work).

Finally the third verification is that when the beam is fully wrapped and conforms to the cam profile, there is no region along the contact where the fourth derivative of the beam deflection is positive

$$\frac{d^4\hat{y}}{dx^4} \le 0 \quad \text{must hold for} \quad 0 \le x \le L \tag{18}$$

This condition ensures that no tensile contact tractions are required to ensure the beam is conformal with the cam shape (reactive compressive contact tractions may be applied by the cam). If indeed it is found that condition (18) is not satisfied then a different design strategy should be used, as described in the next section.

4. Cam-guiding - when the beam has a single contact point with the cam

In this section we analyze the response of a cantilever beam with a guided end, which is bent over a curved cam such that it has a single tangential contact point $(x_c, \hat{y}_c)$ (beside the contact at the clamped edge), as illustrated in Fig. 4. In this sense the cam constrains and guides the deflection of the flexure.

The deflection curve of the beam is given by

$$y = \begin{cases} \left[x^2(3L-2x) - \frac{x^2}{x_c}(6Lx_c - 3x_c^2 - 2Lx)\left(\frac{3L-2x_c}{4L-3x_c}\right)\right]\frac{F}{12E^*I} \\ \qquad + (6Lx_c - 3x_c^2 - 2Lx)\frac{x^2\hat{y}_c}{x_c^3(4L-3x_c)} & 0 \le x \le x_c \\ \left[x^2(3L-2x) - x_c(6Lx - 3x^2 - 2Lx_c)\left(\frac{3L-2x_c}{4L-3x_c}\right)\right]\frac{F}{12E^*I} \\ \qquad + (6Lx - 3x^2 - 2Lx_c)\frac{\hat{y}_c}{x_c(4L-3x_c)} & x_c \le x \le L \end{cases} \tag{19}$$

The slope at $x = 0$ and $x = L$ vanishes and there is continuity of slope and displacement at the contact point x_c where the two domains meet.

By setting $x = L$ we find the transverse force F as a function of the edge deflection $\Delta = y_{(x=L)}$ and the deflection y_c at the contact point

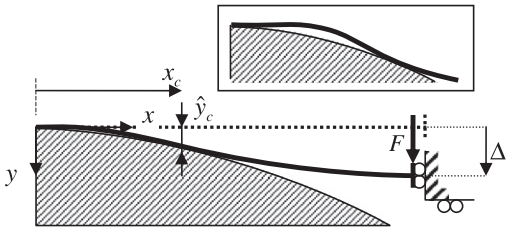

Fig. 4. Schematic model of a clamped-guided beam bent over a cam which has a single contact point $(x_c, \hat{y}_c)$ (beside the contact at the clamped edge).

$$F = \frac{3E^*I}{(L-x_c)^3}\frac{4L-3x_c}{L}\Delta - \frac{1}{x_c}\frac{3L-2x_c}{(L-x_c)^3}3E^*I\hat{y}_c \tag{20}$$

Clearly, when $x_c = 0$ this relation reduces to $F = 12E^*I\Delta/L^3$ which is compatible with (10). The stiffness of the guided end when the beam leans on the cam at point $(x_c, \hat{y}_c)$ is

$$k = \frac{\partial F}{\partial \Delta} = \frac{3E^*I}{(L-x_c)^3}\frac{4L-3x_c}{L} \tag{21}$$

Here we assume that the variation of $\hat{y}_c/x_c$ due to small variations in Δ is negligible (this holds for shallow cams with $d\hat{y}_c/dx_c << 1$). The functional form of the stiffness (21) reflects the fact that the beam is clamped at its origin, and indeed when $x_c = 0$ the stiffness reduces to that of a cantilever beam (Eq. (11)).

For a desired functional form of force $F(\Delta)$, we can use Eq. (21) to derive the guided-edge deflection as function of the contact location $\Delta(x_c)$, and then use Eq. (20) to derive the cam profile $\hat{y}_c(x_c)$.

As in the case of the cam-wrapping design method (Section 3), there are three issues that have to be cleared. The first two are the issues of strength and the validity of the Euler–Bernoulli beam theory. The third essential verification is that throughout the loading process the beam is never predicted to penetrate the cam.

In the next section we try both design methods (i.e., cam-wrapping and cam-guiding) to design a cam that linearizes the response of the gap-closing parallel-plates actuator.

5. Specific cam design

We now present the design of a cam-wrapping suspension that will reconstruct the force–displacement law (5), which is rewritten here

$$F(\Delta) = \frac{\beta\Delta^2}{(g-\Delta)^2} \tag{22}$$

This force–displacement law is plotted as a solid line in Fig. 5. The stiffness associated with this force–displacement law is

$$k = \frac{dF}{d\Delta} = \frac{2\beta g\Delta}{(g-\Delta)^3} \tag{23}$$

Evidently, for very small loading the stiffness vanishes, which means that initially the beam has to have infinite length. Since this is not possible, we will pre-load the system with a constant stiffness (dashed line in Fig. 5) up to a specific point Δ_0 on the force–displacement curve. Since we already know that with a linear spring the system will lose its stability when the displacement reaches a third of the gap (i.e., $\Delta = g/3$), we will choose $\Delta_0 < g/3$.

The response of the parallel-plates actuator for which we design this nonlinear suspension, is illustrated in Fig. 6. Up to the edge

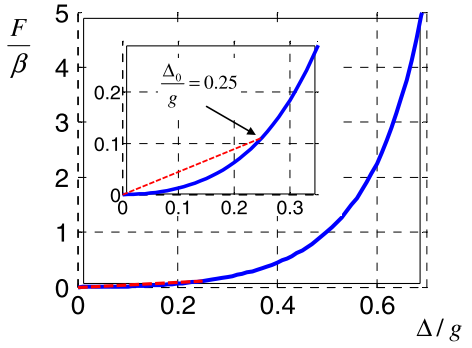

Fig. 5. Illustration of the force–displacement law (22) for the case $\Delta_0 = g/4$. The inset is an enlargement of the linear pre-loading response.

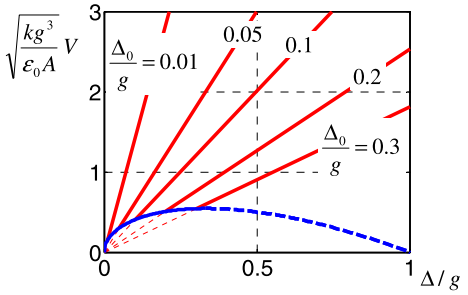

Fig. 6. Predicted voltage-displacement relation for various values of Δ_0.

displacement of Δ_0 the voltage will be given by (3) (curved solid line in Fig. 6), and from this edge-deflection on, the voltage will be linearly proportional to the displacement (oblique straight solid lines for various values of Δ_0/g).

Consider the linear pre-loading up to edge-deflection Δ_0 (inset of Fig. 5). Up to this point the stiffness of the suspension is given by

$$k_{0-} = \frac{F_0}{\Delta_0} = \frac{\beta\Delta_0}{(g-\Delta_0)^2} = \frac{12E^*I}{L^3} \tag{24}$$

From which we deduce that

$$\beta = \frac{12E^*I}{L^3}\frac{(g-\Delta_0)^2}{\Delta_0} \tag{25}$$

From this point on, the required stiffness is given by (23) and therefore further loading from edge-deflection Δ_0 must occur with stiffness

$$k_{0+} = \frac{2\beta g\Delta_0}{(g-\Delta_0)^3} = \frac{2g}{(g-\Delta_0)}\frac{12E^*I}{L^3} \tag{26}$$

5.1. Cam-wrapping design

Comparing the desired initial wrapping stiffness (26) with (17), it follows that when $\Delta = \Delta_0$ the beam has to be instantaneously shortened from its initial unwrapped length L, to a length of

$$L_0 = L - x_{c0} = L\sqrt[3]{\frac{1}{2}\left(1-\frac{\Delta_0}{g}\right)} \tag{27}$$

Since $\Delta_0 < g/3$, we find that $x_{c0}/L \le 1 - \sqrt[3]{1/3} \approx 0.307$.

To design a specific spring for a given parallel-plate actuator with a given gap g, we begin by setting the length of the unwrapped beam, which we expect to be much larger than the gap ($L >> g$). We next choose the desired initial loading point Δ_0 ($\Delta_0 < g/3$) on the equilibrium curve shown in Fig. 6, and determine the point x_{c0} from Eq. (27). Based on the mechanical restoring force F_0 we desire at this point (e.g. Eq. (1)), we use Eq. (24) to determine the second moment of the beam cross-section. Once this has been set, we can substitute x_{c0}, F_0, and E^*I in Eq. (10) and determine the beam deflection-curve up to point x_{c0}. For elegance, we may decide that the cam will be in contact with the beam in this entire region. Accordingly the cam profile in the region $0 \le x \le x_{c0}$ is given by

$$\hat{y}(x) = \frac{F_0}{E^*I}\left(\frac{Lx^2}{4} - \frac{x^3}{6}\right) = \Delta_0\left(3\frac{x^2}{L^2} - 2\frac{x^3}{L^3}\right) (\text{for } 0 \le x \le x_{c0}) \tag{28}$$

And the cam height and slope at x_{c0} are therefore

$$\hat{y}_0 = \Delta_0\left(3\frac{x_{c0}^2}{L^2} - 2\frac{x_{c0}^3}{L^3}\right) \tag{29}$$

$$\hat{y}_0' = 6\frac{\Delta_0}{L}\left(\frac{x_{c0}}{L} - \frac{x_{c0}^2}{L^2}\right) \tag{30}$$

Notice that for $F = F_0$ the beam is in contact with the cam in the region $0 \le x \le x_{c0}$ but no contact traction is applied between the beam and cam.

From this point on we proceed with the cam design using numerical computation. First though, we can derive an analytic expression for the edge deflection as function of the point of last contact x_c. Substituting the desired stiffness (23) with β given by (25) into (17), yields a cubic equation for $\Delta(x_c)$. Two solutions of this cubic equation are non-physical (i.e., $\Delta > g$), and the one physically meaningful solution is

$$\frac{\Delta(x_c)}{g} = 1 + \frac{1}{3} Z_1^{-1/3} \Gamma_1^2 \left(1 - \frac{x_c}{L}\right)^2 - \Gamma_1 \left(1 - \frac{x_c}{L}\right) Z^{1/3} \tag{31}$$

where

$$Z = \frac{1}{2}\left(1 + \sqrt{1 + \frac{4}{27}\Gamma_1^3 \left(1 - \frac{x_c}{L}\right)^3}\right), \quad \Gamma_1 = \sqrt[3]{2\frac{(1-\Delta_0/g)^2}{\Delta_0/g}} \tag{32}$$

We can now substitute $\Delta(x_c)$ from (31) into Eq. (16) which is rewritten in the form

$$\left.\frac{d^2\hat{y}}{dx^2}\right|_{x_c} = \frac{6}{(L-x_c)^2}\left(\Delta(x_c) - \hat{y}(x_c) - \frac{2}{3}\left.\frac{d\hat{y}}{dx}\right|_{x_c}(L - x_c)\right) \tag{33}$$

This second order differential equation can be integrated with initial conditions (29) and (30).

5.2. Cam-guiding design

Substituting the desired stiffness (23) with β given by (25), into the stiffness of the cam-guided beam (21) yields

$$8g\frac{\Delta}{\Delta_0}\frac{(g-\Delta_0)^2}{(g-\Delta)^3} = L^2\frac{4L-3x_c}{(L-x_c)^3} \tag{34}$$

This bi-cubic equation may be solved for $x_c(\Delta)$ or solved for $\Delta(x_c)$. Solving (34) for $x_c(\Delta)$ yields two complex solution which are not physical (i.e., $x_c > L$) and one physically meaningful solution

$$x_c = L\left(1 - \frac{Z_2}{2\Gamma_2} - \frac{2}{Z_2}\right) \tag{35}$$

where

$$Z_2 = \sqrt[3]{\left(1 - \sqrt{1 - \frac{4}{\Gamma_2}}\right)4\Gamma_2^2}, \quad \Gamma_2 = 8\frac{\Delta}{\Delta_0}\frac{(1-\Delta_0/g)^2}{(1-\Delta/g)^3} \tag{36}$$

By setting $\Delta = \Delta_0$ this equation can be used to determine the initial contact point x_{c0} (notice that this initial contact point is not the same as for the cam-wrapping design). As in the previous subsection, for elegance, we may decide that in the region $0 \le x \le x_{c0}$ the cam will have the same profile as the beam, that is will be given by Eq. (28).

As for the profile of the guiding cam beyond this point (i.e., $x > x_{c0}$), solving (34) for $\Delta(x_c)$ yields two complex solutions which are not physical (i.e., $\Delta > g$) and one physically meaningful solution

$$\Delta = g\left(1 + \frac{Z_3}{6\Gamma_3} - \frac{2}{Z_3}\right) \tag{37}$$

where

$$Z_3 = 3\cdot\sqrt[3]{\left(-1 + \sqrt{1 + \frac{4}{27\Gamma_3}}\right)4\Gamma_3^2}, \quad \Gamma_3 = \frac{\Delta_0/g}{8(1-\Delta_0/g)^2}\frac{4 - 3x_c/L}{(1-x_c/L)^3} \tag{38}$$

We can now substitute $\Delta(x_c)$ from (37) into (20), and with (22) and (25) get an equation that yields the cam profile $\hat{y}_c(x_c)$

$$\hat{y}_c = \Delta(x_c)\frac{x_c}{3L-2x_c}\left(\frac{4L-3x_c}{L} - 4\frac{(L-x_c)^3}{L^3}\frac{\Delta(x_c)}{\Delta_0}\frac{(g-\Delta_0)^2}{(g-\Delta(x_c))^2}\right) \text{ for } x_c > x_{c0} \tag{39}$$

6. Experimental validation

A macro scale test device was manufactured to verify the theoretical analysis, as shown in Fig. 7. To implement a guided end condition, two identical cams were stacked, and two identical beams were connected at their far edge to a rigid connector. The beams and cams were bolted together and fastened to a thick plate which was used to clamp the device to an Instron test machine.

The cams and connector were machined from 6061 aluminum, and the beams were cut from a thin 5052 aluminum sheet. The mechanical properties of the beams and the geometrical parameters of the test device appear in Table 1.

The load was applied to the rigid connector at the guided edge with an intermediating steel bearing-ball to relieve axial loads on the beams (Fig. 8). The beam ends were connected to the load cell in a way that enabled to apply negative loads necessary to compensate for sagging due to the beam and connector weight (this sagging is visible in Fig. 7).

The cams shown in Fig. 7 were designed assuming conformal wrapping of the beams. Namely, using the parameters in Table 1., from Eq. (27) it was found that the initial contact point is at $x_{c0} = 8.37\cdot10^{-2}[m]$. So the cam profile up to this point is given by Eq. (28). The cam profile from this point on was computed by integrating Eq. (33) with initial conditions (29) and (30).

However, verification revealed that condition (18) is not satisfied and in fact, there must be disconnection between the cams and wrapped beams. Conformal wrapping would have required that the cam applies a tensile traction of up to 32.5 kPa to the wrapped beam. This traction is small in comparison to the stresses induced by bending in the beam, but it is nonetheless not physical. We have verified that a cam that would have been designed according to Eq. (39) would have satisfied the conditions detailed

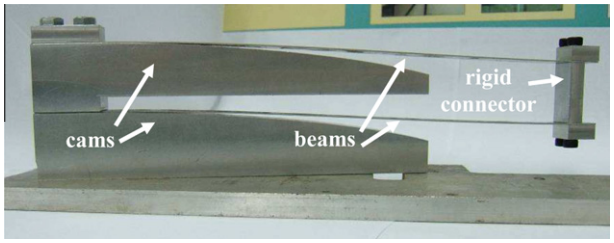

Fig. 7. The macro-scale test device. Two beams with a rigid edge connector were used to ensure a guided-edge condition.

Table 1
Material and geometrical parameters of the test device.

$E = 70.3\cdot10^9[Pa]$	Young's modulus of the beams
$\sigma_{yield} = 214\cdot10^6[Pa]$	Tensile Yield Strength
$\nu = 0.33$	Poisson's ratio of the beams
$g = 7.5\cdot10^{-2}[m]$	Initial gap
$\Delta_0 = g/4$	Initial loading
$L = 30\cdot10^{-2}[m]$	Beam length
$h = 9.15\cdot10^{-4}[m]$	Beam height
$w = 2\cdot10^{-2}[m]$	Beam width

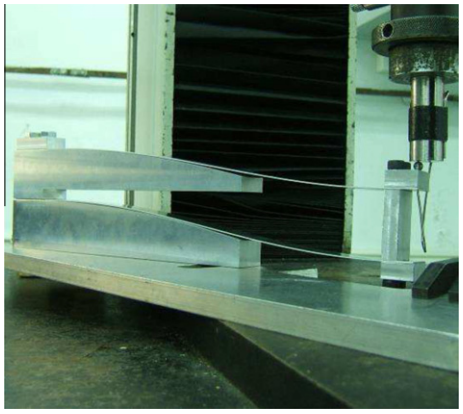

Fig. 8. The test device under loading. A steel bearing-ball was introduced between the parallel flat surfaces connector and load cell to relieve axial loads on the beam.

at the end of Section 4, and therefore would have been a perfect cam.

However, we had already fabricated the cams according to the cam-wrapping design, so we decided to proceed and test them. Though the design of these cams was not perfect for linearizing the response of the gap-closing parallel-plates actuator in a microsystem, they may nevertheless be used to demonstrate the concept of using a cam and beam structure to achieve a nonlinear spring with increasing stiffness.

To theoretically predict the experimental measurements we computed the force–displacement relation for these cams assuming the beam flexures are guided by them, with a single point of contact between each cam and beam. To this end, we computed the slope of the beams by differentiating (19) with respect to x. Then we set $x = x_c$ in this derivative to obtain the slope $\hat{y}'_c$ at the contact point, which was given as function of x_c, $\hat{y}_c$, and F. From this we extracted the force F as function of x_c, $\hat{y}_c$, and $\hat{y}'_c$, which were all known for the fabricated cams. Next, we substituted this force into (20) and extracted the edge displacement Δ as function of x_c, $\hat{y}_c$, and $\hat{y}'_c$. It was verified that the fabricated cams may indeed serve as guides for the flexures without any predicted overlaps between cam and beam. This was very fortunate, for if the verification failed, it is not at all clear that the design problem has a solution, and in any case a third and different design methodology had to be developed.

Fig 9 presents typical experimental measurements (measurements were recorded through 20 cycles of loading and unloading with no observable hysteresis). Since it was difficult to accurately determine when the beam was perfectly straight, the measured load and displacement were each shifted by a constant so that the kink in the measured curve fits its predicted location.

During the experiments the computed maximal stresses in the loaded spring were lower than the yield stress of the beam.

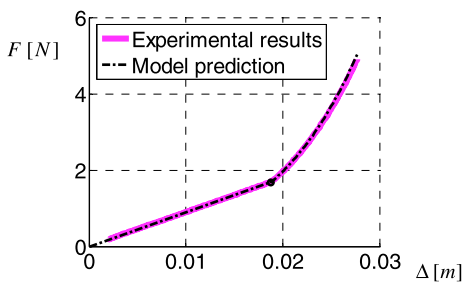

Fig. 9. Typical force–displacement measurements. No hysteresis was observed during 20 cycles of loading/unloading.

Overall, the measurements are in good agreement with the model predictions, and we consider this as confirmation of the design concept of nonlinear springs.

7. Summary and discussion

We have proposed a method for designing nonlinear elastic springs with monotonically increasing stiffness. The necessity in such nonlinear springs is motivated by the nonlinear response of electrostatic gap-closing actuators. The specific spring considered in this work is intended to increase the dynamic range of the parallel-plates electrostatic actuator and furthermore to force a linear relation between applied voltage and resulting displacement. Proof of concept micro devices are currently in production.

Two methods were presented to design cams assuming two possible scenarios. The first scenario assumes that the wrapped section is in full contact with the cam, and the second scenario assumes that there is a single contact point between the beam flexure and the cam. In either case, the validity of the proposed solution must be a posteriori verified. In the case of conformal wrapping it must be verified that tensile reactive contact tractions are not necessary to hold the beam in contact with the cam. In the later case it must be verified that none of the predicted deformed shapes of the beam intersects the cam.

Due to the complexity of the design process it is impossible to a priori know which case is relevant for a given desired force–displacement law. In fact, it may be that for a specific desired spring with a specific desired force–displacement law, each of these scenarios will be applicable to a distinctively different domain of the response. Furthermore, it may be that both design methods would fail to produce a desired nonlinear spring (e.g. verifications of both considered methodologies fail). Since we had a specific type of nonlinear response in mind, and since for this response the cam-guiding design is applicable, we have not considered other cases. We consider the good agreement between experiments and model prediction as validation of the design concept of nonlinear springs.

References

Burns, D.M., Bright, V.M., 1997. Nonlinear flexures for stable deflection of an electrostatically actuated micromirror. In: Proceedings of SPIE: Microelectronics Structures and MEMS for Optical Processing III, vol. 3226, pp. 125–135.

Cortopassi, C., Englander, O., 2001. Nonlinear springs for increasing the maximum stable deflection of MEMS electrostatic gap closing actuators. UC Berkeley. Available from: <http://www-bsac.eecs.berkeley.edu/~pister/245/project/CortopassiEnglander.pdf>.

Deutsch, E.R., Bardhan, J.P., Senturia, S.D., Hocker, G.B., Youngner, D.W., Sinclair, M.B., Butler, M.A., A large-Travel vertical planar actuator with improved stability. In: IEEE-TRANSDUCERS 2003, Boston, 2003, pp. 352–355.

Elata, D., 2006. Modeling the electromechanical response of electrostatic actuators. In: Leondes, C.T. (Ed.), MEMS/NEMS: handbook techniques and applications, Sensors and Actuators, vol. 4. Springer, New York, pp. 93–119.

Elata, D., Hirshberg, A., 2006. A novel method for measuring the strength of microbeams. J. Microelectromech. Sys. 15, 396–405.

Hung, E.S., Senturia, S.D., 1999. Extending the travel range of analog-tuned electrostatic actuators. J. Microelectromech. Syst. 8, 497–505.

Liu, C., 2006. Foundations of MEMS. Pearson Prentice Hall, Upper Saddle River, NJ.

Love, A.E.H., 1944. A Treatise on the Mathematical Theory of Elasticity. Dover Publications, New York.

Madou, M.J., 2011. Fundamentals of Microfabrication and Nanotechnology. CRC Press, Boca Raton, Fla.

Maluf, N., Williams, K., 2004. An Introduction to Microelectromechanical Systems Engineering. Artech House, Boston.

Marxer, C., Manzardo, O., Herzig, H.P., Dandliker, R., De-Rooij, N., An electrostatic actuator with large dynamic range and linear displacement-voltage behavior for a miniature spectrometer. Transducers '99, Sendai, Japan, 1999, pp. 786–789.

Nadal-Guardia, R., Brosa, A.M., Dehe, A., 2003. Constant charge operation of capacitor sensors based on switched-current circuits. IEEE Sens. J. 3, 835–842.

Nadal-Guardia, R., Dehe, A., Aigner, R., Castaner, L.M., 2002. Current drive methods to extend the range of travel of electrostatic microactuators beyond the voltage pull-in point. J. Microelectromech. Syst. 11, 255–263.

Osterberg, P.M., Senturia, S.D., 1997. M-TEST: a test chip for MEMS material property measurement using electrostatically actuated test structures. J. Microelectromech. Sys. 6, 107–118.

Tang, W.C., Nguyen, T.C.H., Howe, R.T., 1989. Laterally driven polysilicon resonant microstructures. Sensor Actuat. 20, 25–32.

Younis, M.I., Nayfeh, A.H., 2003. A study of the nonlinear response of a resonant microbeam to an electric actuation. Nonlinear Dyn. 31, 91–117.